Ordered magnetic frustration. IV. The two magnetic structures of the inverse weberite $Fe_2F_5(H_2O)_2$: an example of the thermal evolution of the frustration character

1986 J. Phys. C: Solid State Phys. 19 1081

(http://iopscience.iop.org/0022-3719/19/8/007)

J. Phys. C: Solid State Phys. **19** (1986) 1081–1095. Printed in Great Britain

Ordered magnetic frustration: IV. The two magnetic structures of the inverse weberite $Fe_2F_5(H_2O)_2$: an example of the thermal evolution of the frustration character

Y Laligant†, M Leblanc†, J Pannetier‡ and G Ferey†§

† Laboratoire des Fluorures et Oxyfluorures Ioniques (U.A. CNRS No 449), Faculté des Sciences, Université du Maine, Route de Laval, 72017 Le Mans Cedex, France

‡ Institute Laüe–Langevin Grenoble, Avenue des Martyrs 156X, 38042 Grenoble Cedex, France

Received 26 April 1985

Abstract. The nuclear and the two magnetic structures of the ferrimagnetic (T_c = 48(1) K) inverse weberite $Fe_2F_5(H_2O)_2$ were solved by neutron powder diffraction experiments at 60, 30 and 4.2 K respectively. The room temperature structure proposed by Hall *et al* is confirmed at 60 K and hydrogen atoms are located (O–H = 0.944(8) Å; H–O–H = 111.68(9)°). Below T_c, magnetisation data indicate a change in the magnetic structure at 26(1) K. This transition is confirmed by neutronic thermodiffractometry. Above and below this temperature, the magnetic and nuclear cells are identical. At 30 K (space group Imma) all the Fe^{3+} spins (μ = 2.8(1) μ_B) are parallel to [010] (F_y mode), whereas Fe^{2+} moments (μ = 3.8(1) μ_B) lie in the (100) plane (F_y G_z mode). Below 26 K, the magnetic symmetry becomes monoclinic (I 2/b); at 4.2 K, μ_{Fe}^{3+} = 4.9(3) μ_B, μ_{Fe}^{2+} = 3.8(3) μ_B and the canting mode is $F_xF_yG_z$ on each site; the antiferromagnetic mode G_z of Fe^{3+} becomes predominant. This peculiarity is analysed in terms of the strength of the magnetic interactions and topological frustration. The thermal variation of the orientation of the moments is also described.

1. Introduction

We recently introduced (Ferey *et al* 1985a) the concept of ordered magnetic frustration from the study of some 3d transition metal fluorides containing either one (Leblanc *et al* 1984, 1986) or two metallic species (Ferey *et al* 1977, 1985a, b, Leblanc *et al* 1984) which occupy two distinct crystallographic sites.

It is now well known (Toulouse 1977) that frustration occurs when the metallic network, in antiferromagnetic interaction, forms triangular cycles. We have shown that according to the nature of the 3d cations and, consequently, to the strength of the exchange interactions, several arrangements of the spins can result from the frustration: two orthogonal magnetic sublattices of M^{2+} and M^{3+} (in $Mn^{2+}Cr^{3+}F_5$ (Ferey *et al* 1977) and $NH_4Fe^{2+}Fe^{3+}F_6$ (Ferey *et al* 1985) idle spin behaviour for one lattice (in $Fe^{2+}Fe_2^{3+}F_8(H_2O)_2$ (Leblanc *et al* 1984)) or three 120° antiferromagnetic sublattices when a single cationic species is present (HTB-FeF_3 (Leblanc *et al* 1984, 1986)).

§ Author for correspondence.

0022-3719/86/081081 + 15 $02.50

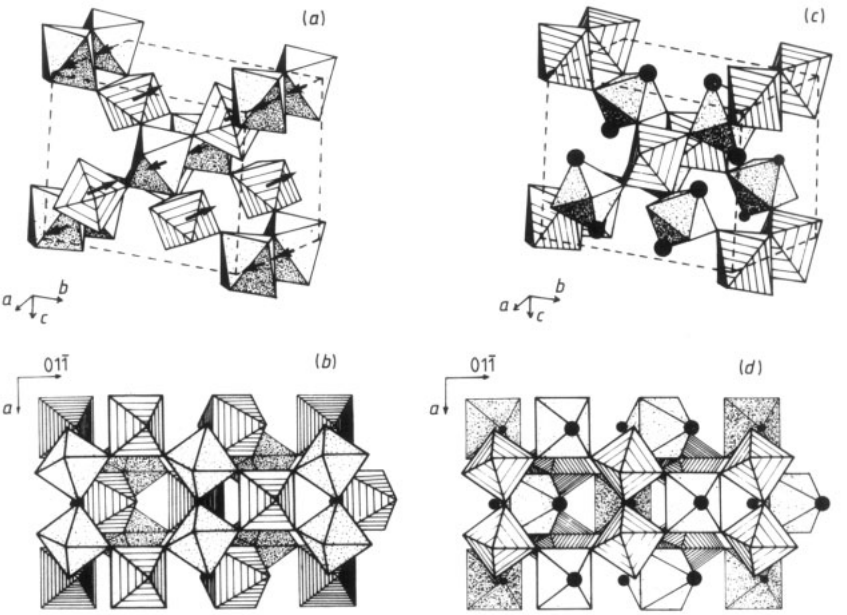

Figure 1. (*a*) Perspective view of the orthorhombic weberite Na_2NiFeF_7 (from Haegele *et al* (1978); Fe^{3+} octahedra are hatched). (*b*) (011) HTB planes in Na_2NiFeF_7. Fe^{3+} octahedra are hatched. (*c*) Perspective view of $Fe^{2+}Fe^{3+}F_5(H_2O)_2$. For the sake of comparison with Na_2NiFeF_7, the origin is shifted by $\boldsymbol{a}/2$ with respect to the original structure (Haegele *et al* 1978). Fe^{3+} octahedra are hatched. H_2O molecules are noted by full circles. (*d*) HTB planes in $\square_2Fe^{2+}Fe^{3+}F_5(H_2O)_2$.

This last structure is built from hexagonal tungsten bronze (HTB) planes (Magneli 1953) of corner sharing octahedra. This arrangement, which is topologically propitious to frustration effects, is encountered in other structures like orthorhombic (Byström 1944, Haegele *et al* 1978, Guisepetti and Tadini 1978, Knop *et al* 1982) (figure 1(*a*)) or trigonal weberites (Verscharen and Babel 1978). In both structures, the HTB planes are built from *trans*-chains of corner sharing $M^{2+}F_6$ octahedra linked by isolated $M^{3+}F_6$ octahedra (figure 1(*b*)). Other $M^{2+}F_6$ octahedra ensure the connection of two HTB layers by sharing two corners with each plane. When these corners are in the *trans*-position, o-weberite is formed; *cis*-linkage leads to t-weberite.

Neutron diffraction studies by Heger on the o-weberites Na_2NiFeF_7 and Na_2NiAlF_7 (Heger and Viebahn-Hansler 1972, Heger 1973) showed that the observed ferrimagnetic behaviour of Na_2NiFeF_7 ($T_c = 90$ K) results from a frustration of Ni^{2+}–Ni^{2+} coupling. In Na_2NiAlF_7, the chains of Ni^{2+} are antiferromagnetically coupled ($T_N = 18$ K) as predicted by the Kanamori–Goodenough rules (Goodenough 1968), whereas in Na_2NiFeF_7 parallel spins of Ni^{2+} lie along [100], the subnetwork of Fe^{3+} being ferromagnetic and antiparallel to Ni^{2+} spins (figure 1(*a*)). This was explained (Tressaud and Dance 1971, Tressaud *et al* 1974) by the strength of the Ni^{2+}–Fe^{3+} coupling as compared to the weak Ni^{2+}–Ni^{2+} interaction. This obliges Ni^{2+} ions to adopt a 'ferromagnetic' arrangement, which corresponds to a frustration of their usual antiferromagnetic coupling.

We observed that the structure of the ferrimagnet ($T_c = 48$ K) $Fe^{2+}Fe^{3+}F_5(H_2O)_2$ (Hall *et al* 1977, Walton *et al* 1977, Jones and Dawson 1978, Laligant *et al* 1986) can be

described as an inverse weberite $\square_2Fe^{2+}Fe^{3+}F_5(H_2O)_2$: M^{2+} and M^{3+} positions are inverse of those which exist in Na_2NiFeF_7, and H_2O molecules belong to the isolated Fe^{2+} octahedra (figure 1(*c*)). Consequently, the strongest interaction Fe^{3+}–Fe^{3+} (which is predicted as exclusively antiferromagnetic (Goodenough 1968) being in the chains (figure 1(*d*)), one may assume that the frustrated arrangment of the spins will be different in Na_2NiFeF_7 and $Fe_2F_5(H_2O)_2$. In addition, the accident observed by Mössbauer spectroscopy in the thermal variation of the hyperfine field of Fe^{3+} at 26 K (Imbert *et al* 1976) led us to study the magnetic structure of $Fe_2F_5(H_2O)_2$ and its thermal evolution by neutron diffraction.

The format of this paper is as follows. We first give a brief description of the experimental procedures in § 2; in § 3 we present the results of magnetic measurements and finally, in § 4 we describe the nuclear and magnetic structures and the thermal variation of the magnetic moments.

2. Experimental details

Crystals of $Fe_2F_5(H_2O)_2$ were obtained, using a modification of the original synthesis (Brauer and Eichner 1958). After reacting iron wire with 49% aqueous HF, the liquid is kept in a Teflon beaker at constant temperature. The evaporation leads to the crystallisation of single crystals of $Fe_2F_5(H_2O)_2$. The main impurities are β-$FeF_3.3H_2O$ at low temperature, and FeF_2 at high temperature. The best yield (95%) is obtained by operating at 110 °C for 1 h.

Between 4.2 and 300 K, the susceptibility was measured on powdered crystals by the Faraday method; a vibrating sample magnetometer with a field reversal unit was used to obtain the magnetisation data in the same temperature range (up to 19 kOe) and hysteresis loops.

Neutron diffraction patterns were collected on the D1B and D1A powder diffractomers of the high-flux reactor of the Institut Laüe–Langevin using wavelengths of 2.522 and 1.909 Å respectively. The sample, prepared by grinding single crystals, was contained in a cylindrical vanadium can (diameter 15 mm for D1A, 10 mm for D1B) held in a vanadium tailed liquid helium cryostat. The high flux and good low angle resolution of D1B allow fast data collection for moderately complex structues; it was used to study the thermal evolution of the pattern in the range 4.2 to 50 K. Diffraction patterns ($20° < 2\theta < 92°$) were collected every 2 K in 6 min. The high resolution of D1A was used to obtain extensive and accurate data at three charactristic temperatures over a larger angular range ($6° < 2\theta < 117°$). The 60 K pattern was collected to locate the hydrogen atoms in the nuclear cell and check the absence of any structural phase transition between room temperature and the Curie temperature ($T_c = 48(1)$K); two other diffraction patterns at 30 K and 4.2 K were recorded to determine the two magnetic structures which exist in the two temperature ranges 4.2–26 K and 26–48 K.

The diffraction patterns were analysed by the Rietveld method (Rietveld 1969) as modified by Hewat (Hewat 1973). Integrated intensities were determined from the thermodiffractogram (see figure 4) by fitting the shape of the Bragg peaks to Gaussians and the background to a first-order polynomial (the INTEGR program, by P Wolfers 1975). The nuclear scattering lengths and magnetic form factors were taken from Koester and Rauch (1979) and Watson (1961) respectively. Absorption corrections were applied (Hewat 1979) and Bertaut's representation theory was used to construct the models of magnetic structures (Bertaut 1963).

3. Magnetic study

Reproducible measurements were obtained on several samples, from different preparations. The ferrimagnetism of $Fe_2F_5(H_2O)_2$ is confirmed by the existence of a hysteresis loop which was studied at several temperatures between 4.2 and 48 K. Two examples are given on figure 2(*a*). They display a relatively large coercive field, close to 4 kOe at low temperature. When T increases, H_c abruptly drops to 1 kOe in the vicinity of 25 K; above this temperature, it decreases monotonically till 48 K. The $\sigma(H)$ versus T curves, measured at decreasing fields (figure 2(*b–c*)) increase from 52 K, reach a maximum in

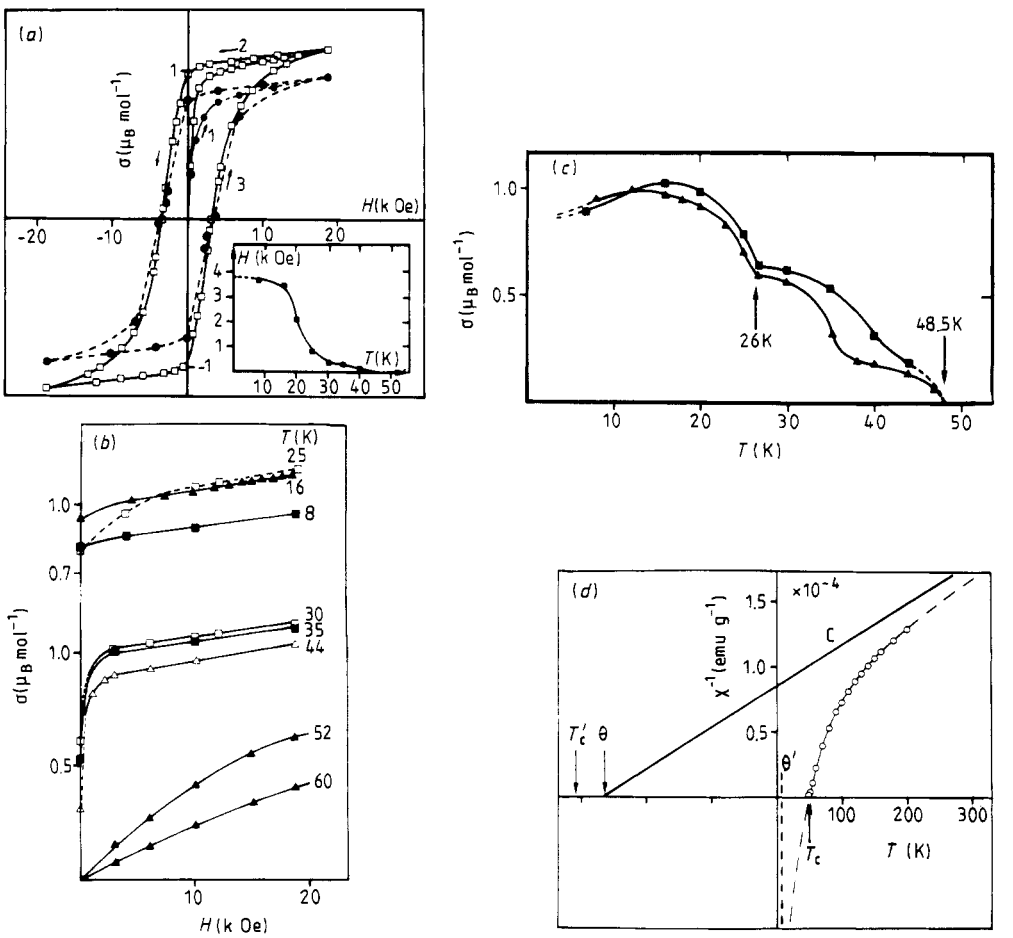

Figure 2. (*a*) Hysteresis loops of $Fe_2F_5(H_2O)_2$ at 8 K (●) and 16 K (○). The first magnetisation curves (1) are drawn up to 19 kOe. It is followed by a decrease of the magnetic field down to −19 kOe (2), then by an increase up to the maximum field (3). (Insert: thermal evolution of the coercive field H_c). (*b*) $\sigma(H)$ curves at $T > 25$ K and $T < 25$ K. The measurements were performed at decreasing fields. (*c*) Thermal evolution of the remanent magnetisation (see text). ■, σ_r hysteresis loops; ▲, σ_r heating at zero field. For curve ▲, σ_R was measured every 1 min. (*d*) $\chi^{-1}(T)$ curve for $Fe_2F_5(H_2O)_2$. The full curve is least-squares fitted to the experimental points (○). Numerical values of the fitted constants appear in table 1.

the 25–30 K temperature range, and then decrease, as already mentioned by Walton *et al* (1977). In addition, the thermal variation of remanent magnetisation deduced from these curves shows a singularity around 26 K; the same feature is also observed by studying the variation with temperature of the remanent magnetisation from its 4.2 K value under 19 kOe (figure 2(*c*)).

All these observations are consistent with the previously described discontinuity in the temperature variation of the hyperfine field of Fe^{3+} (Imbert *et al* 1976) and imply a change in the magnetic structure of $Fe_2F_5(H_2O)_2$ at 26 K.

The Curie temperature has been accurately determined from susceptibility data at 8 kOe by least-squares fitting the experimental points to the following expression (Smart 1956) (figure 2(*d*)):

$$1/\chi = \frac{(T - T_c)(T - T_c')}{C(T - \theta)}.$$

The calculated values are in agreement with Walton's results (table 1).

Table 1. Comparison of the results from the magnetic studies on $Fe_2F_5(H_2O)_2$.

	Walton *et al* (1977)	Jones and Dawson (1978)	This work
T_c (K)	48.5	48.5	48.5(1)
θ_p (K)	−179	−138	−256.1(4)
C_M (exp.)	6.74	7.03	6.70(4)
C_M (calc.)	7.38	7.38	7.38
μ_{eff} (exp.)	7.34	7.5	7.32(3)
μ_{eff} (calc.)	7.68	7.68	7.68
T_c'	−200.9	—	−308.8
θ'	25.8	—	6.43
$\sigma_{sat}(\mu B)$	1.2	0.82	0.85(2)

4. Neutron diffraction

4.1. Nuclear structure at 60 K

The nuclear structure was refined in space group Imma (table 2) using 69 peaks resolved by the program into 122 *hkl* triplets ($6 < \theta < 117°35'$). The final values of cell parameters and atomic coordinates are given in table 3. The incoherent scattering for hydrogen atoms gives rise to a relatively high background in the diffraction patterns and leads to relatively high R profiles. The isotropic thermal parameters were fixed to 0.13, 0.36, 0.17 and 1.30 $Å^2$ for iron, fluorine, oxygen and hydrogen respectively.

Parts of the (001) and (010) projections of the structure at 60 K are shown in figure 3(*a*, *b*). The non-hydrogen atoms do not exhibit large deviations from their 300 K positions. As expected, the corresponding distances (table 4) are shortened with respect to room temperature values. The geometry of the water molecules bonded to Fe^{2+} is close to the ideal one. The hydrogen atoms form strong hydrogen bonds (d_{H-F} = 1.894 Å) with the Fl atoms which are shared between Fe^{2+} and Fe^{3+} octahedra.

Table 2. *R* factors for the refinement of the neutron diffraction at 60, 30 and 4.2 K.

	60 K	30 K	4.2 K
Expected *R* (%)	8.96	11.40	6.74
Profile *R*	13.29	14.01	11.81
Weighted profile *R*	10.16	11.23	9.33
Nuclear *R*	5.68	6.51	4.17
Magnetic *R*	—	9.22	7.81

Table 3. Refined cell parameters and atomic positions. ESD are given in parentheses and refer to the last digit.

T (K)	*a* (Å)	*b* (Å)	*c* (Å)
300	7.477(1)	10.862(2)	6.652(2)
60	7.472(1)	10.928(1)	6.606(2)
30	7.469(1)	10.927(1)	6.602(1)
4.2	7.470(1)	10.930(1)	6.603(1)

Atom	Site	*x*	*y*	*z*
Fe^{2+}	4a	0	0	0
Fe^{3+}	4c	$\frac{1}{4}$	$\frac{1}{4}$	$\frac{1}{4}$
		0.2032(3)	0.1266(2)	0.0511(3)
F_1	16j	0.2034(2)	0.1257(3)	0.0496(1)
		0.2029(2)	0.1252(7)	0.0507(1)
				0.3364(6)
F_2	4e	0	$\frac{1}{4}$	0.3368(2)
				0.3347(2)
			0.5659(4)	0.1962(5)
O	8h	$\frac{1}{2}$	0.5658(4)	0.1994(2)
			0.5653(4)	0.1974(2)
		0.3954(5)	0.5875(4)	0.1242(5)
H	16j	0.3941(7)	0.5878(7)	0.1188(8)
		0.3933(3)	0.5871(3)	0.1207(2)

† The first, second and third lines refer respectively to the 60, 30 and 4.2 K refinements.

4.2. Neutron thermo-diffractometry below T_c

The diffraction patterns, collected at constant temperature every 2 K between 4.2 and 48 K are displayed in figure 4. At all temperatures, the magnetic and the nuclear cells are identical. At 26 K, (noted by arrows on figure 4) a change in the magnetic structure is clearly shown. In the range 48 to 26 K, the intensities of some nuclear peaks increases and a few new (*hk*0) magnetic reflections appear in the pattern. They all correspond to the condition $h, k = 2n$, consistent with the group Imma. The existence of the (200) reflection is of peculiar interest for the discussion of the low temperature magnetic structure. At 26 K, a new magnetic reflection (110), forbidden in the space group Imma, appears which indicates a change in the magnetic space group, although the cell parameters are not modified. The magnetic intensities of some nuclear peaks abruptly

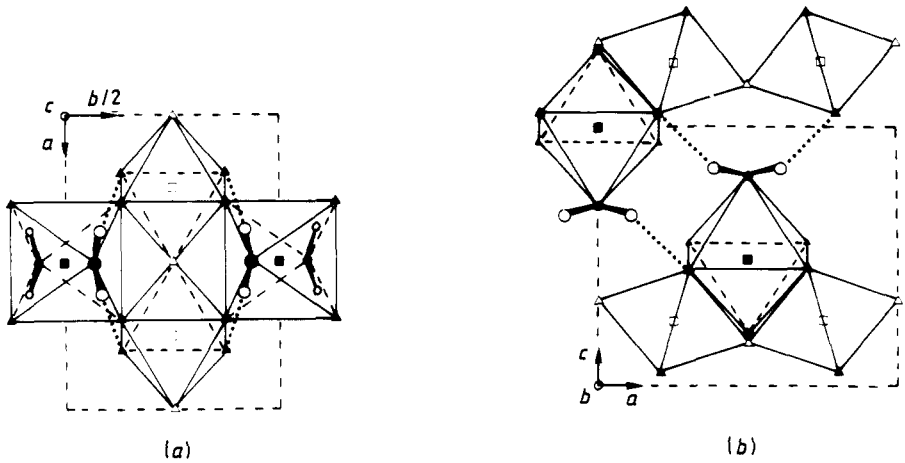

Figure 3. (001) (*a*) and (010) (*b*) projections of a part of the nuclear structure of $Fe_2F_5(H_2O)_2$ at 60 K. They show the water molecules and the hydrogen bonds with F_1^- ions. ■ Fe^{2-}, z = $\frac{1}{2}$; □ Fe^{3-}, $z = \frac{1}{4}$; ▲ F_1^-; △ F_2; ●● O, z = 0.81 and 0.19; ○○ H, z = 0.88 and 0.13.

Table 4. Interatomic distances (Å) and bond angles (deg) at 60 K.

Fe^{2-} octahedron			
Fe–F_1	4 × 2.080(1)	F_1–Fe–F_1	85.88(7) 94.12(7)
Fe–O	2 × 2.132(3)	F_1–Fe–O	86.33(8) 93.67(8)
F_1–F_1	4 × 2.848(4)		
F_1–O	4 × 2.848(3) 4 × 2.871(4)	Fe–O–H	120.50(11)
Fe^{3-} octahedron			
Fe–F_1	4 × 1.925(3)	F_1–Fe–F_1	89.53(7) 90.47(7)
Fe–F_2	2 × 1.953(7)		
F_1–F_1	2 × 2.697(4) 2 × 2.719(3)	F_1–Fe–F_2	88.52(6) 91.21(6)
F_1–F_2	4 × 2.700(4) 4 × 2.770(3)		
Superexchange angles and metal–metal distances			
Fe^{3-}–F_2–Fe^{3-}	146.02(13)	Fe^{2-}–F_1–Fe^{3-}	135.44(12)
Fe^{3-}–Fe^{3-}	3.736(4)	Fe^{2-}–Fe^{3-}	3.698(9)
Water molecule			
O–H	2 × 0.944(8)	H–O–H	111.68(11)
H–H	1.563(7)		
H . . . F_1	1.894(6)		

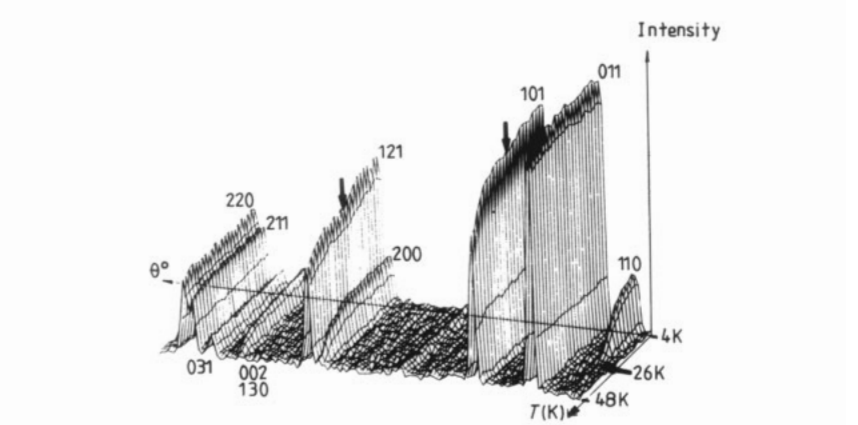

Figure 4. Thermal evolution of the neutron powder diffraction pattern ($10° \leq 2\theta \leq 36°$) between 4 and 48 K. Note the change of intensity of some reflections (noted by arrows) at 26 K.

increase, whereas some others are not affected. The thermal variation of the integrated intensities of the significant peaks are shown in figure 5(*a*). As has already been pointed out, the magnetic nature of the anomaly observed at 26 K is corroborated by the Mössbauer results (Imbert *et al* 1976) (figure 5(*b*)). A detailed study of the magnetic structure at 30 and 4.2 K was undertaken to further investigate this magnetic anomaly.

4.3. The high temperature magnetic structure at 30 K

As mentioned above, the identity of the nuclear and magnetic cells allow Bertaut's macroscopic theory (Bertaut 1963) to be used. $\bar{2}_x$, $\bar{2}_y$ $\bar{1}$ and I translation are taken as the four independent symmetry elements. If $\boldsymbol{R}_i$ and $\boldsymbol{S}_i$ ($i = 1, 4$) are the magnetic moments

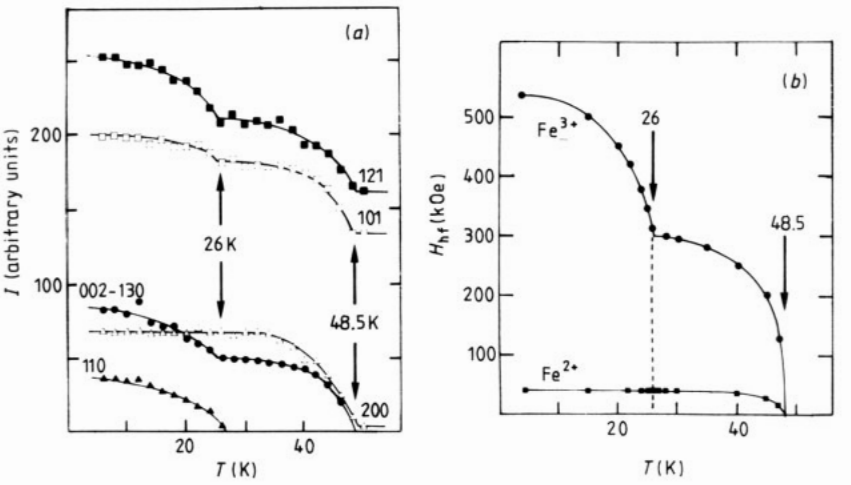

Figure 5. (*a*) Thermal variation of the intensity of some magnetic peaks of $Fe_2F_5(H_2O)_2$, compared to (*b*) the thermal variation of the hyperfine field of Fe^{3+} and Fe^{2+} deduced from Mössbauer data (Imbert *et al* 1976).

Table 5. Coordinates of the magnetic ions R_i (Fe^{3+}) and S_i (Fe^{2+}) and part of the irreducible representation of Fe^{3+} and Fe^{2+} in the Imma group. This part corresponds to the representations compatible with a magnetisation on both sublattices.

	Fe^{3+}				Fe^{2+}		
R_1	$\frac{1}{4}$	$\frac{1}{4}$	$\frac{1}{4}$	S_1	0	0	0
R_2	$\frac{3}{4}$	$\frac{1}{4}$	$\frac{1}{4}$	S_2	0	$\frac{1}{2}$	0
R_3	$\frac{3}{4}$	$\frac{3}{4}$	$\frac{3}{4}$	S_3	$\frac{1}{2}$	$\frac{1}{2}$	$\frac{1}{2}$
R_4	$\frac{1}{4}$	$\frac{3}{4}$	$\frac{3}{4}$	S_4	$\frac{1}{2}$	0	$\frac{1}{2}$
Mode	x	y	z		x	y	z
$\Gamma_1(++++)$	.	G_y	.		G_x	.	.
$\Gamma_2(-+++)$	.	F_y	.		.	F_y	G_z
$\Gamma_3(+-++)$	F_x	.	G_z		F_x	.	.
$\Gamma_4(--++)$	G_x	.	F_z		.	G_y	F_z

of Fe^{3+} and Fe^{2+} corresponding to the atomic coordinates reported in table 5, it is possible to define in each sublattice four linear combinations of the moments

$$F = M_1 + M_2 + M_3 + M_4$$

$$G = M_1 - M_2 + M_3 - M_4$$

$$C = M_1 + M_2 - M_3 - M_4$$

$$A = M_1 - M_2 - M_3 + M_4$$

($M = R, S$) which represent the ferromagnetic and the antiferromagnetic modes of coupling. The base vectors, in the irreducible representation of space group Imma, lead to 16 modes but only four of them are compatible with the magnetisation of both Fe^{3+} and Fe^{2+} sublattices (table 5).

Table 6. Refined magnetic moments (in μ_B) at 30 K (upright) and 4.2 K (italic).

Atom	M_x	M_y	M_z	M
R_1	—	+2.80(10)	—	2.80(10)
	−0.7(2)	*3.12(10)*	*3.73(8)*	*4.9(3)*
R_2	—	+2.80(10)	—	2.80(10)
	−0.7(2)	*3.12(10)*	*−3.73(8)*	*4.9(3)*
R_3	—	+2.80(10)	—	2.80(10)
	−0.7(2)	*3.12(10)*	*+3.73(8)*	*4.9(3)*
R_4	—	+2.80(10)	—	2.80(10)
	−0.7(2)	*3.12(10)*	*−3.73(8)*	*4.9(3)*
S_1	—	−3.52(8)	−1.60(8)	3.86(16)
	1.6(2)	*−3.4(1)*	*−1.0(2)*	*3.80(3)*
S_2	—	−3.52(8)	+1.60(8)	3.86(16)
	1.6(2)	*−3.4(1)*	*+1.0(2)*	*3.80(3)*
S_3	—	−3.52(8)	−1.60(8)	3.86(16)
	1.6(2)	*−3.4(1)*	*−1.0(2)*	*3.80(3)*
S_4	—	−3.52(8)	+1.60(8)	3.86(16)
	1.6(2)	*−3.4(1)*	*+1.0(2)*	*3.80(3)*

The best fit ($R = 9.22\%$) between observed and calculated magnetic intensities (a list can be obtained on request to G Ferey) corresponds to the Γ2 mode with signs $+F_y$ for the Fe^{3+} component and $-F_y - G_z$ for the Fe^{2+} ones. All other combinations of signs led to an increase of the R factor. The components of the magnetic moments M ($M = R, S$) on the axes of the cell are listed in table 6. The comparison of the observed and calculated profiles appear in figure 6(a). The main feature of this structure is the parallel alignment of Fe^{3+} spins along $\boldsymbol{b}$ (figure 7(a)); this point will be further discussed in the conclusion.

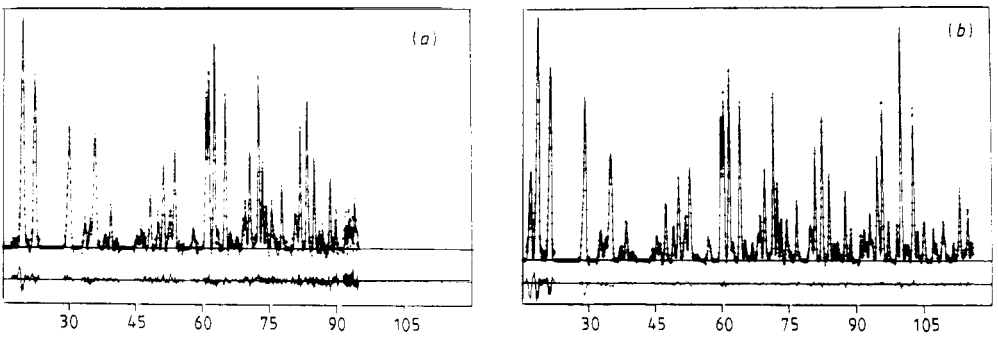

Figure 6. Calculated (solid line) and observed (crosses) neutron diffraction patterns of $Fe_2F_5(H_2O)_2$ at 30 K (a) and 4.2 K (b). The bottom line is the difference pattern (same scale).

4.4. The low temperature magnetic structure at 4.2 K

The existence of the (110) purely magnetic reflection below 26 K is still compatible with a body-centred lattice but excludes the Imma group; this suggests the space group Imm2, if the orthorhombic symmetry is preserved. However, this implies a translation of the origin of the nuclear cell by a vector $(0, -\frac{1}{4}\boldsymbol{b}, -\frac{1}{4}\boldsymbol{c})$. The corresponding new positions and the two Bertaut modes which describe the simultaneous magnetisation of the two sublattices are listed in table 7. However, both models yield unacceptably high magnetic

Table 7. Magnetic modes corresponding to the simultaneous magnetisation of the Fe^{3-} (R_i) and Fe^{2-} (S_i) sublattices (Imm2).

	Fe^{3-}				Fe^{2-}		
$\boldsymbol{R}_1$	$\frac{1}{4}$	0	0	$\boldsymbol{S}_1$	0	0.25	0.75
$\boldsymbol{R}_2$	$\frac{3}{4}$	0	0	$\boldsymbol{S}_2$	0	0.75	0.75
$\boldsymbol{R}_3$	$\frac{3}{4}$	$\frac{1}{2}$	$\frac{1}{2}$	$\boldsymbol{S}_3$	$\frac{1}{2}$	0.75	0.75
$\boldsymbol{R}_4$	$\frac{1}{4}$	$\frac{1}{2}$	$\frac{1}{2}$	$\boldsymbol{S}_4$	$\frac{1}{2}$	0.25	0.25
Mode	x	y	z		x	y	z
2zm I							
$\Gamma_1(+++)$	.	G_y	.		G_x	G_y	F_z
$\Gamma_2(-++)$	F_x	.	G_z		F_x	F_y	G_z

Table 8. Results in the Imm2 group (T = 4.2 K; moments in μ_B).

Mode	R_x	R_y	R_z	$\|\boldsymbol{R}_1\|$	S_x	S_y	S_z	$\|\boldsymbol{S}_1\|$	R_{nuc}	R_{mag}
Γ_1	.	3.17	.	3.17	0.41	1.31	3.45	3.77	7.50	19.7
Γ_2	−1.41	.	3.27	3.57	1.65	−3.03	0.22	3.45	5.60	16.1

Table 9. Magnetic modes of Fe^{3+} ($\boldsymbol{R}_i$) and Fe^{2+} ($\boldsymbol{S}_i$) in the non-standard I112/b space group.

	Fe^{3+}				Fe^{2+}		
$\boldsymbol{R}_1$	$\frac{1}{4}$	$\frac{1}{4}$	$\frac{1}{4}$	$\boldsymbol{S}_1$	0	0	0
$\boldsymbol{R}_2$	$\frac{3}{4}$	$\frac{1}{4}$	$\frac{1}{4}$	$\boldsymbol{S}_2$	0	$\frac{1}{2}$	0
$\boldsymbol{R}_3$	$\frac{3}{4}$	$\frac{3}{4}$	$\frac{3}{4}$	$\boldsymbol{S}_3$	$\frac{1}{2}$	$\frac{1}{2}$	$\frac{1}{2}$
$\boldsymbol{R}_4$	$\frac{1}{4}$	$\frac{3}{4}$	$\frac{3}{4}$	$\boldsymbol{S}_4$	$\frac{1}{2}$	0	$\frac{1}{2}$
Modes	x	y	z		x	y	z
I $\tilde{2}\tilde{z}$ 1							
$\Gamma_1(+-+)$	F_x	F_y	G_z		F_x	F_y	G_z
$\Gamma_2(+++)$	G_x	G_y	F_z		G_x	G_y	F_z
$\Gamma_3(--+)$	C_x	C_y	A_z		.	.	.
$\Gamma_4(-++)$	A_x	A_y	C_z		.	.	.
$\Gamma_5(---)$	.	.	.		C_x	C_y	A_z
$\Gamma_6(-+-)$	.	.	.		A_x	A_y	C_z
$\Gamma_7(+--)$	.	.	.		.	.	.
$\Gamma_8(++-)$	.	.	.		.	.	.

R (table 8); more specifically, the calculated intensities of the (200) and (222) reflections are much smaller than the observed values.

The subgroups of Imm2 were then systematically investigated using the *International Tables of Crystallography* (Hann 1984). The only satisfactory result (R_{mag} = 0.078) is obtained with the Γ_1 mode of the non-standard space group I 112/b (C2/c), the cation positions being the same as in Imma (tables 6 and 9). $\tilde{2}\tilde{z}$, $\bar{1}$ and I translation were taken as independent symmetry elements. This model, which gives a good fit to the experimental profile (figure 6(*b*)), leads to a rather complex magnetic structure which is presented in figure 7(*b*). Each sublattice belongs to the $F_xF_yG_z$ mode but the components of each metallic network are antiparallel. Compared to the 30 K situation a ferromagnetic component appears along x for Fe^{2+}, the y and z values being only slightly modified, as is the value of $\mu_{Fe^{2+}}$. This last result corroborates the previous Mössbauer results; however, the main feature is the appearance for Fe^{3+} of an antiferromagnetic mode along z, coupled with a weak ferromagnetism along x and a small increase of the F_y value. This leads to an enhancement of the magnetic moment of Fe^{3+} to 4.9 μ_B, close to its ideal value. Figure 8 and table 10 summarise the canting of the spins at 30 and 4.2 K in the bitriangular frustrating unit 2 Fe^{3+} ($\boldsymbol{R}_1$, $\boldsymbol{R}_2$) + 2 Fe^{2+}($\boldsymbol{S}_3$, $\boldsymbol{S}_4$). $\boldsymbol{R}_i$, $\boldsymbol{S}_i$ angles decrease from 30 to 4.2 K. Simultaneously, the $\boldsymbol{R}_1 \cdot \boldsymbol{R}_2$ angle between Fe^{2+} moments increases from 0 to ~100° in the same temperature range, but is still far from the antiferromagnetic arrangement which would be obtained if frustration was absent. The present angle can be compared to the value of 151°, obtained at 4.2 K for Fe^{3+} spins (μ = 4.12 μ_B) in $NH_4Fe^{2+}Fe^{3+}F_6$ (Ferey *et al* 1985).

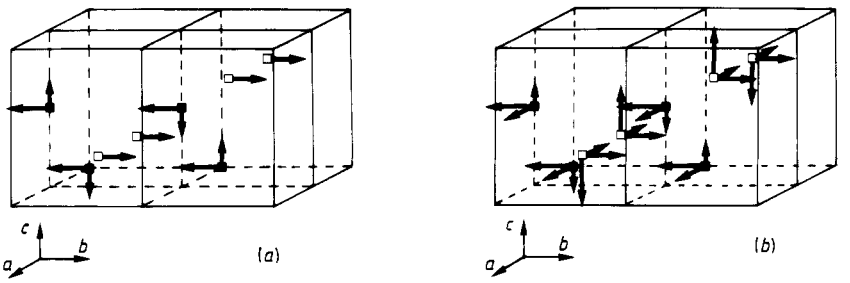

Figure 7. Spin configuration at 30 K (*a*) and 4.2 K (*b*) (■ Fe^{2-}, □ Fe^{3-}).

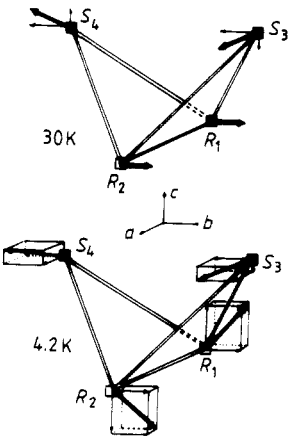

Figure 8. Detail of the magnetic structure which shows the orientation of the moments towards the bitriangle.

Table 10. Canting angles (deg) between spins of Fe^{3-} and Fe^{2-} at 30 and 4.2 K ($\boldsymbol{R}_i$ and $\boldsymbol{S}_i$ refer to atomic coordinates of table 6).

	30 K	4.2 K
R_1R_2	0	101.1
S_3S_4	48.9	46.6
$R_1S_4 = R_2S_3$	155.6	114.7
$R_1S_3 = R_2S_4$	155.6	144.0

4.5. Thermal variation of the magnetic moments between 4.2 and 48 K

The temperature variation of the orientation of the magnetic moments was calculated from the D1B patterns (figure 4). This evolution can be described either in polar (figure 9(*a*, *b*)) or cartesian coordinates (figure 9(*c*)). Both the orientation and the modulus of each moment show singularities at 26 K. From these calculations we determined the contribution to the magnetic dipolar energy at each temperature. The lattice summation was carried out in real space within a sphere of 100 Å radius; it shows that the Fe^{2+}–Fe^{3+} interaction is predominant (figure 10).

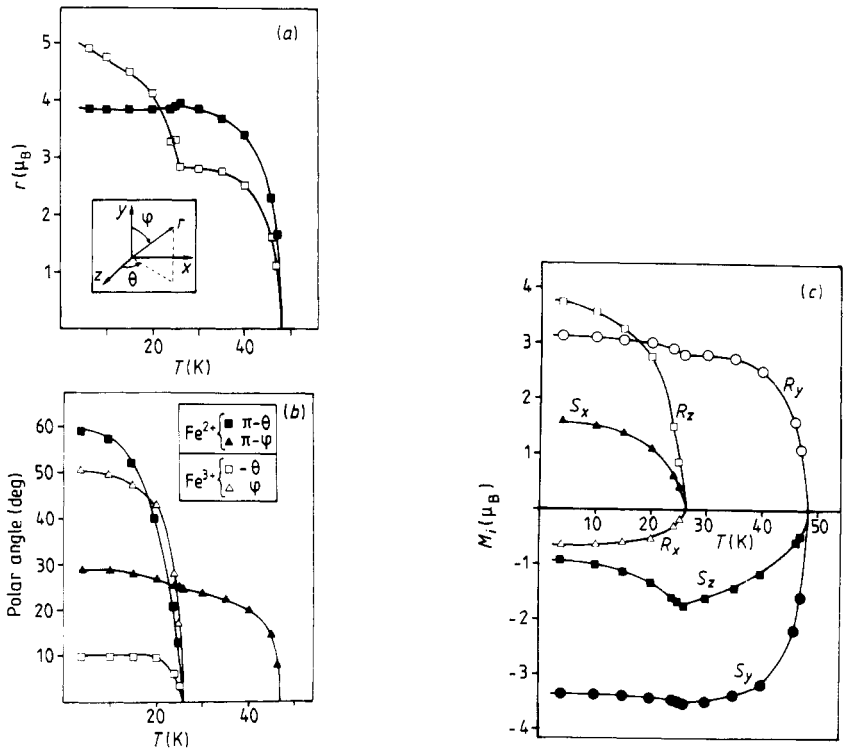

Figure 9. Temperature variation of (*a*) the modulus of the magnetic moments (■ Fe^{2+}, □ Fe^{3+}), (*b*) the angles θ and φ between the moments and the crystallographic axes, (*c*) the components of each magnetic moment along the crystallographic axes.

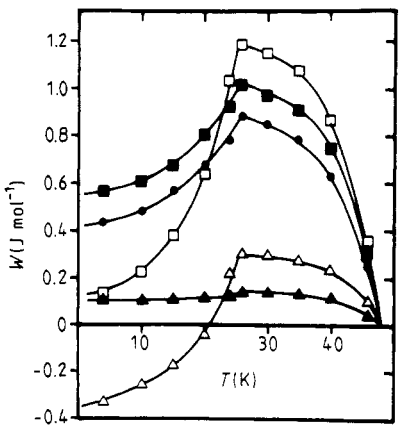

Figure 10. Thermal evolution of the magnetic dipolar energy $W\,i/i, j, (i+j)$ created on a site i by the other i, j or $(i+j)$ moments: ■ $Fe^{2+}/Fe^{2+} + Fe^{3+}$ □ $Fe^{3+}/Fe^{2+} + Fe^{3+}$, ▲ Fe^{2+}/Fe^{2+}, △ Fe^{3+}/Fe^{3+} ● Fe^{2+}/Fe^{3+} or Fe^{3+}/Fe^{2+}.

5. Conclusion

In contradiction to predictions of the Kanamori–Goodenough (KG) theory, our results show that, when a frustrating triangular cationic sub-network of a structure is occupied

in an ordered way by two kinds of cations, one of them being anisotropic, the frustrated arrangement of the spins is governed by two factors:

(i) the crystal field and/or superexchange anisotropy;
(ii) the thermal variation of the strength of the different magnetic interactions.

In $Fe_2F_5(H_2O)_2$, the application of the KG rules would suggest a strong antiferromagnetic superexchange coupling for Fe^{3+}–Fe^{3+} and a weaker one for Fe^{2+}–Fe^{3+} interactions, as already observed in $NH_4Fe_2F_6$ (Ferey *et al* 1985a) and $Fe_3F_8(H_2O)_2$ (Leblanc *et al* 1984). However, previous Mössbauer studies (Imbert *et al* 1976) and the present investigation show that between 26 and 48 K, the anisotropy of Fe^{2+} governs the magnetic structure. The corresponding moments quickly reach their maximum value (3.8 μ_B), and, under their influence, Fe^{3+} spins which are only weakly coupled adopt a parallel arrangement which frustrates their 'natural' antiferromagnetic coupling; the strongest interaction then occurs between Fe^{2+} and Fe^{3+}.

This is the very case which occurs in the weberite Na_2NiFeF_7 where the parallel disposition of Ni^{2+} spins corresponds to a frustration of their coupling.

However, for the latter compound, the same situation still exists at the lowest temperatures, owing to the small moment of Ni^{2+}. In $Fe_2F_5(H_2O)_2$, as the temperature decreases, the Fe^{3+}–Fe^{3+} interaction grows stronger and tends to favour antiferromagnetic coupling. This begins to occur at 26 K, when the G_z component of Fe^{3+} appears. Below this temperature the Fe^{3+}–Fe^{3+} coupling becomes predominant and obliges the moments to adopt a different arrangement. However, the difference between Fe^{3+}–Fe^{3+} and Fe^{2+}–Fe^{3+} superexchange interactions is not large enough to lead to a strict antiparallelism of the spins of Fe^{3+} and at 4.2 K, their angle is still ~100°.

Two related studies concerning $MnFeF_5(H_2O)_2$, in which anisotropy is absent, and $ZnFeF_5(H_2O)_2$, which is not frustrated, are in progress.

Acknowledgments

The authors are very indebted to Dr M Guillot (CNRS Grenoble) and to Dr P J Brown (ILL Grenoble) for many fruitful discussions and for their critical reading of the manuscript. For parts I–III of this series, see Ferey *et al* (1977, 1985a, b).

References

Bertaut E F 1963 in *Magnetism III* ed. G T Rado and H Suhl
Brauer G and Eichner M 1958 *Z. Anorg. Allgem. Chem.* **296** 13
Byström A 1944 *Arkiv Kemi. Min. Geol.* **18B** 10
Ferey G, De Pape R and Boucher B 1977 *Acta Crystallogr.* B **34** 1084
Ferey G, Leblanc M, De Pape R and Pannetier J 1985a *Inorganic Fluorides: Chemistry and Physic.* ed. P Hagenmuller (New York: Academic)
—— 1985b *Solid State Commun.* **53** 559
Giusepetti G and Tadini C 1978 *Tschermaks Min. Petr. Mitt.* **25** 57
Goodenough J B 1963 *Magnetism and the Chemical Bond* (New York: Interscience)
Haegele R, Verscharen W, Babel D, Dance J M and Tressaud A 1978 *J. Solid State Chem.* **24** 77
Hall, W, Kim S, Zubieta J, Walton E G and Brown D B 1977 *Inorg. Chem.* **16** 1884
Hann T (ed.) *International Tables for X-ray Crystallography* (Dordrecht: Reidel)
Heger G 1973 *Int. J. Magn.* **5** 119
Heger G and Viebahn-Hansler R 1972 *Solid State Commun.* **11** 1119

Hewat A W 1973 *Harwell Rep.* AERE R 7350
—— 1979 *Acta Crystallogr.* A **35** 248
Imbert P, Jehanno G, Macheteau Y and Varret F 1976 *J. Physique* **37** 969
Jones Jr E R and Dawson R 1978 *J. Chem. Phys.* **69** 3289
Knop O, Cameron T S and Jochem K 1982 *J. Solid State Chem.* **43** 213
Koester L and Rauch H 1981 *IAEA Contract* 2517/RB
Laligant Y, Pannetier J, Labbe P and Ferey G 1986 *J. Solid State Chem.* **62** at press
Leblanc M 1984 *Thèse* Université du Maine, Le Mans
Leblanc M, Ferey G, Calage Y and De Page R 1984 *J. Solid State Chem.* **53** 360
Leblanc M, Pannetier J and Ferey G 1986 *Solid State Commun.* at press
Magneli A 1953 *Acta Chem. Scand.* **7** 315
Rietveld H M 1969 *J. Appl. Cryst.* **2** 65
Smart J S 1966 *Effective Field Theories of Magnetism* (Philadelphia: Saunders)
Toulouse G 1977 *Comm. Phys.* **2** 115
Tressaud A and Dance J M 1971 *Adv. Inorg. Chem.* **20** 133
Tressaud A, Dance J M, Portier J and Hagenmuller P 1974 *Mater. Res. Bull.* **9** 121
Verscharen W and Babel D 1978 *J. Solid State Chem.* **24** 405
Walton E G, Brown D B, Wong H and Reiff W H 1977 *Inorg. Chem.* **16** 2425
Watson R E and Freeman J 1961 *Acta Crystallogr.* **14** 27